PHYSICS

Spectral multiplexing of telecom emitters with stable transition frequency

Alexander Ulanowski[1], Benjamin Merkel[1], Andreas Reiserer[1,2]*

In a quantum network, coherent emitters can be entangled over large distances using photonic channels. In solid-state devices, the required efficient light-emitter interface can be implemented by confining the light in nanophotonic structures. However, fluctuating charges and magnetic moments at the nearby interface then lead to spectral instability of the emitters. Here, we avoid this limitation when enhancing the photon emission up to 70(12)-fold using a Fabry-Perot resonator with an embedded 19-micrometer-thin crystalline membrane, in which we observe around 100 individual erbium emitters. In long-term measurements, they exhibit an exceptional spectral stability of <0.2 megahertz that is limited by the coupling to surrounding nuclear spins. We further implement spectrally multiplexed coherent control and find an optical coherence time of 0.11(1) milliseconds, approaching the lifetime limit of 0.3 milliseconds for the strongest-coupled emitters. Our results constitute an important step toward frequency-multiplexed quantum-network nodes operating directly at a telecommunication wavelength.

INTRODUCTION

Quantum networks can solve tasks and allow their users to interact in ways that are not possible using present-day technology (*1*). Pioneering experiments have used atoms trapped in vacuum (*2*, *3*), quantum dots (*4*), and color centers in diamond (*5*). To access the full potential of quantum networks, these prototypes need to be scaled to longer distances and larger qubit numbers. To this end, one needs to overcome the inefficiency and imperfections of photon transmission over large distances, which can be achieved by the techniques introduced in the seminal quantum repeater proposal (*6*).

Implementing this and related protocols for distributed quantum computing (*7*, *8*) requires, first, an efficient emitter-photon interface, which can be achieved with optical resonators with small volume and large quality factor (*3*, *4*, *9*). Second, to bridge large distances using optical fibers, the photons should be emitted in (*10*) or converted to (*11*) the minimal-loss wavelength regime around 1550 nm. Third, one needs to operate and control multiple qubits per quantum network node, e.g., by using nuclear spin registers (*12*) or by spectral multiplexing (*13*). Last, these qubits have to emit at a reproducible frequency and maintain their optical coherence during the photon emission, and their ground-state coherence until entanglement with a remote node is reliably established. Combining all of these properties in a single experimental platform is an outstanding challenge.

While efficient light-matter interfaces have been realized in several solid-state platforms using nanophotonic resonators (*4*, *9*, *10*, *13*–*15*), in this approach, the proximity of fluctuating charges and paramagnetic impurities at nearby interfaces leads to noise that is detrimental to the spectral stability of the emitters. Thus, except for a recent work in SiC (*16*), the cavity-enhanced generation of coherent photons has only been achieved with emitters that exhibit a low sensitivity to electric fields due to a zero first-order Stark coefficient that is a result of their symmetry (*17*, *18*). These emitters (*14*, *19*, *20*) did not operate at a telecommunication wavelength and often required dilution refrigerators to ensure coherent operation.

Here, we implement an alternative approach that requires neither insensitive emitters nor millikelvin temperature as it avoids the proximity of interfaces. Thus, it should be applicable to a large variety of emitters and host materials. In our experiment, we place a thin crystalline membrane of erbium-doped yttrium orthosilicate (Er:YSO) in a cryogenic Fabry-Perot resonator (*21*) with a high quality factor of 10^7. Compared to our earlier experiment on ensemble spectroscopy (*22*), we use the same crystal and mirror but a changed mechanical arrangement (see Materials and Methods). Despite the considerable first-order Stark shift of Er:YSO, around 10 kHz/(V*cm) (*23*), we demonstrate coherent emission of single photons with exceptionally narrow spectral diffusion linewidth. As the latter is much smaller than the frequency difference between individual dopants caused by inhomogeneous strain in the crystal, many emitters can be individually addressed and coherently controlled in the same resonator by spectral multiplexing (*13*).

Among all investigated photon emitters that host long-lived qubits (*24*, *25*), erbium is the only one that exhibits a coherent (*26*) optical transition in the minimal-loss band of fiber-optical telecommunication, around 1536 nm. Together with the demonstrated second-long ground-state coherence in high magnetic fields (*27*), this is a unique advantage toward the realization of global quantum networks. In recent experiments, single erbium dopants have been resolved in a nanophotonic resonator (*10*), and up to four dopants have been controlled simultaneously (*13*). However, in these experiments, the emitters were close to an interface. Thus, fast dephasing has broadened the emission linewidth to >10 MHz, even at a temperature of 0.5 K. This has hampered the optical control of a larger number of qubits and the optical entanglement of erbium dopants. We demonstrate that this obstacle is overcome in our approach.

RESULTS

Single-dopant spectroscopy

The experimental setup of our Fabry-Perot resonator is shown in Fig. 1A. It is described in detail in (*22*) and in Materials and Methods. The emission of the cavity-coupled erbium dopants is excited by

[1]Max-Planck-Institut für Quantenoptik, Quantum Networks Group, Hans-Kopfermann-Strasse 1, D-85748 Garching, Germany. [2]Technical University of Munich, TUM School of Natural Sciences and Munich Center for Quantum Science and Technology (MCQST), James-Franck-Str. 1, D-85748 Garching, Germany.
*Corresponding author. Email: andreas.reiserer@mpq.mpg.de

faint laser pulses (that typically contain $\lesssim 10^4$ photons), resonant with the 1536.49-nm transition between the lowest crystal field levels of erbium in YSO, and polarized along the D_2 axis, as shown in Fig. 1B. The resonant fluorescence is observed using a superconducting nanowire single-photon detector with a quantum efficiency of 20(2)% at a dark count rate of 5(2) Hz. When scanning the excitation laser frequency and the cavity resonance in parallel, we observe many peaks that originate from single dopants located close to the antinodes of the standing wave cavity field (see Fig. 2A). Their emission is enhanced via the Purcell effect (*3*, *4*, *9*) with enhancement factors up to $P = 70(12)$, depending on the dopant position in the cavity mode. These P values, determined from lifetime measurements (see Fig. 2, D and E), are in excellent agreement with the expectation based on the resonator geometry (see Materials and Methods). Assuming a random spatial distribution of emitters in the mode and using the dopant density as the only free parameter, the expected distribution (*22*) of Purcell factors (orange dashed) shows good agreement with the data (blue bars), except that fewer dopants with the highest Purcell factors are observed. We attribute this to a slight detuning between dopants and cavity in this measurement. Dopants with $P \lesssim 10$ are not included because of the finite signal to noise achieved with the used detectors.

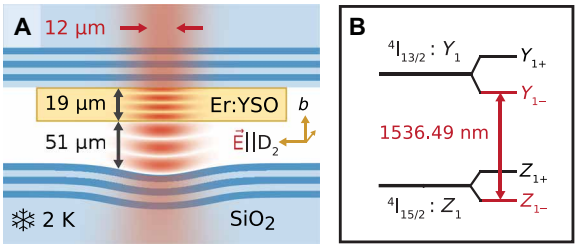

Fig. 1. Setup and level scheme. (**A**) Fabry-Perot cavity (not to scale). A resonator with small mode volume is formed by a flat and a concave glass mirror (blue; bottom and top) with deposited Bragg reflectors (dark blue), confining a stable optical mode (red). Erbium dopants are integrated in a thin, atomically flat crystalline membrane (yellow rectangle). (**B**) Energy level scheme. The studied transition (red) is between the lowest spin and crystal-field levels of the 15/2 and 13/2 manifolds of erbium in YSO.

For $P \gg 1$, the erbium emission is almost fully channeled into the resonator, enabling high photon generation efficiency. In our setup, the probability that a photon leaves through the coupling mirror is 34(3)%, and 63(9)% of these photons are coupled into a single-mode optical fiber. The overall probability to detect an emitted photon in our setup is further reduced to ~2.4% by the finite transmission of the fiber-optical setup of 57(4)% and the detector efficiency. Each of these values may be further improved in the future.

As a single dopant can only emit one photon at a time, on each peak, we observe antibunching when measuring the photon temporal correlation function $g^{(2)}(\tau)$ (*3*). The latter is measured using a single device, as the dead time of the detector (<0.1 μs) is small compared to the emitter decay (>150 μs). This reduces the dark-count

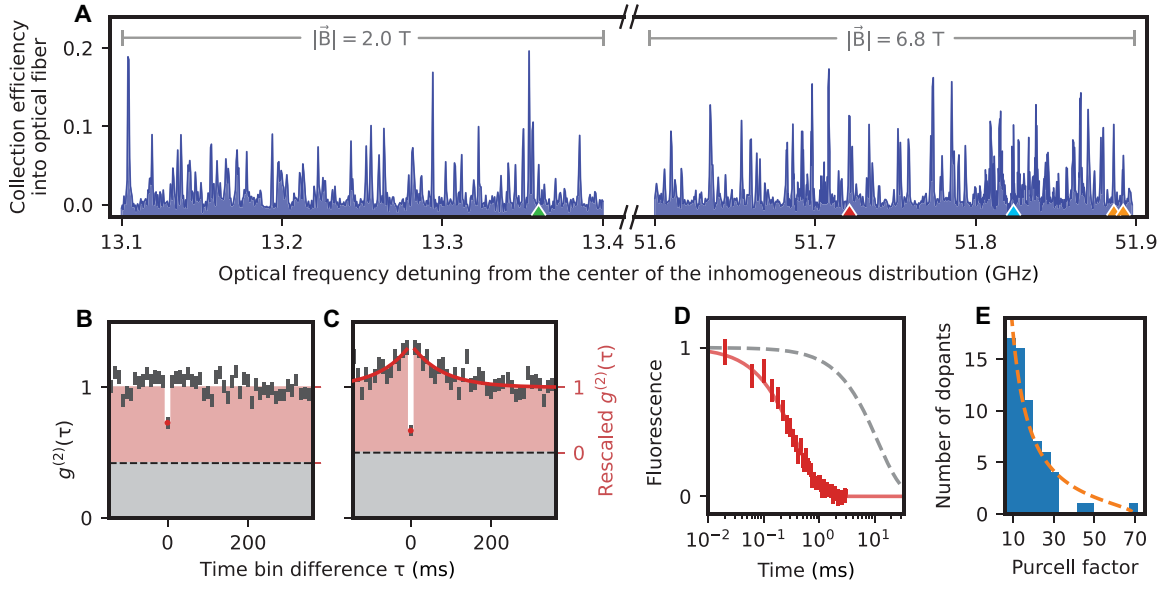

Fig. 2. Cavity-enhanced resonance fluorescence spectroscopy. The error bars denote the 1σ statistical uncertainty. (**A**) Fluorescence spectrum. The resonator is optically excited with chirped laser pulses of 0.5-MHz bandwidth, generated by an acousto-optical modulator to achieve a large inversion probability. With a repetition rate of <2 kHz, the fluorescence is measured as a function of the detuning of the pulse center frequency from the center of the inhomogeneous distribution. Over a large frequency range, individual emitters lead to distinct narrow peaks in the spectrum, whose amplitude reflects the strength of the emitter-cavity coupling. (**B** and **C**) Photon autocorrelation function $g^{(2)}(\tau)$ measured on a randomly chosen peak [red triangle in (A)]; raw data (gray) and background-corrected data (red) with subtracted detector dark count contribution (dashed line). (B) For fixed-frequency Gaussian excitation pulses with 0.55-MHz (FWHM) bandwidth, a rescaled $g^{(2)}(0) < 0.5$ indicates that a peak in the spectrum originates from a single emitter. (C) When the excitation bandwidth is reduced to 0.28 MHz, the smaller contribution of weakly coupled dopants gives a reduced coincidence probability at zero delay, approaching the dark count level (dashed line). The temporal decay of the bunching observed for short time differences is used to determine the time scale of spectral diffusion, 80(20) ms (red exponential fit curve). (**D**) Purcell enhancement of a randomly chosen single dopant [red triangle in (A)]. The data and fit (red) indicate a 30.0(8)-fold reduction of the lifetime as compared to dopants in bulk YSO (gray dashed line). (**E**) Histogram of the extracted Purcell factors (blue bars) for all prominent peaks between 51.6 and 51.9 GHz in (A) and theoretical expectation (orange dashed line).

contribution but implies $g^{(2)}(\tau)=g^2(-\tau)$. In Fig. 2 (B and C), we exemplarily show the data for a randomly selected well-coupled dopant with an integration window of 500 μs, measured at a repetition rate of 100 Hz. For a perfect emitter and setup, $g^{(2)}(0) = 0$. In the depicted measurement, we observe a finite value of 0.73(4), which is, in parts, explained by dark counts of the detector (dashed line) that could be almost completely eliminated with state-of-the-art superconducting nanowire single-photon detectors that obtain 0.1-Hz dark counts at almost 100% quantum efficiency (*28*). In our experiment, we subtract the independently measured dark count contribution and rescale the data (*29*), finding $g^{(2)}(0) = 0.53(7)$, limited by background emission from other dopants that are close in emission frequency but only weakly coupled to the resonator mode because they are located at its side, or at a node of the standing-wave field. Compared to experiments with nanophotonic resonators (*13*), the increased background originates from the almost thousand-fold larger spectral density of emitters in our experiment. It could thus be reduced or avoided using crystals of lower dopant concentration, potentially even doped only at specific locations. As a straightforward alternative, we reduce the background contribution using excitation pulses of smaller spectral width, e.g., 0.28 MHz in Fig. 2C. Reducing the bandwidth by a factor of two leads to an approximately twofold reduction of the background, which results in $g^{(2)}(0) = 0.34(8)$. This testifies that we indeed observe a single emitter. However, when using narrowband pulses, the excitation probability is diminished if the laser frequency does not precisely match that of the emitter. The latter is not perfectly stable because of the fluctuating magnetic field caused mainly by the nuclear spin bath in YSO. This leads to the observation of bunching when the excitation pulse bandwidth approaches or is reduced below the emitter spectral diffusion linewidth, which will be characterized in more detail below. We observe a characteristic decay constant of 80(20) ms at large magnetic fields, here, 6.8 T.

Thus, the change of the resonance frequency of the dopants happens on a time scale that is slow compared to their lifetime ($\lesssim$0.5 ms). With improved count rates, using fast resonance frequency measurements and feedback [e.g., via Stark-shifting electrodes (*5*, *23*, *30*)], our setup can therefore generate single photons with very narrow linewidth for application in extremely dense wavelength division multiplexing. The limit of the current measurement is the pulse bandwidth of 0.28 MHz, while the ultimate limit is given by the radiative linewidth of 1.1-kHz full width at half maximum (FWHM; for the strongest coupled dopants) or by the emitter dephasing. To quantify the latter, we perform coherent spectroscopy.

Spectrally multiplexed coherent control of individual dopants

To this end, we first establish coherent control over individual dopants by applying laser pulses of constant frequency on resonance with one of the peaks in the spectrum. When the intensity of the Gaussian excitation pulses of 1-μs duration (FWHM) is scanned, the fluorescence signal after the pulse shows coherent Rabi oscillations on all investigated dopants, which demonstrates the ability to selectively initialize, control, and read the state of individual dopants via frequency multiplexing. In Fig. 3A, we again show exemplary data of a randomly chosen emitter (blue triangle in Fig. 2A). We attribute the observed damping to a fluctuation of the pulse intensity that is caused by fluctuations of the cavity resonance frequency between repetitions of the experiment, with a typical oscillation time

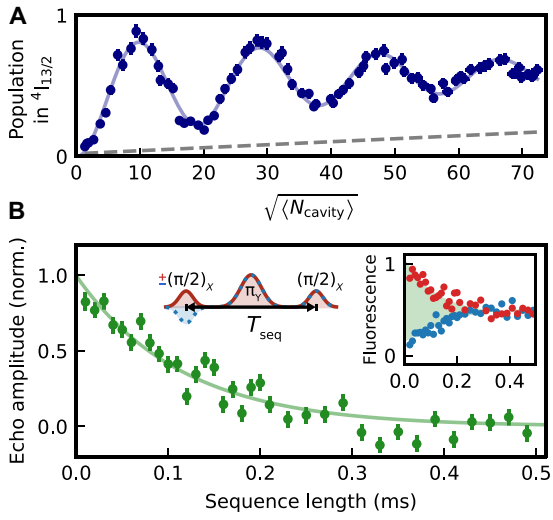

Fig. 3. Optical coherence. (**A**) An excitation laser pulse of varying intracavity mean photon number $\langle N_{\mathrm{cavity}}\rangle$ is applied to excite the fluorescence of a single dopant. The observation of Rabi oscillations proofs coherent control. The observed decay is well fit by a model (blue line) that includes cavity resonance fluctuations and the excitation of a background of weakly coupled dopants (gray dashed line). (**B**) Optical spin echo spectroscopy. To measure the optical coherence time, a laser pulse that performs a π/2 rotation is applied to the dopant. After a delay time of $T_{\mathrm{seq}}/2$ (left inset), a π pulse cancels the effect of a static detuning between dopant and laser. Last, another π/2 pulse is applied. The decay of the difference signal (main panel; green data and exponential fit) between measurements with unchanged (right inset; red) and inverted (blue) phase of the first pulse gives an optical coherence time of 0.11(1) ms. The error bars denote the 1σ statistical uncertainty.

scale of 0.1 ms and an amplitude up to 6 MHz (FWHM) in the used closed-cycle cryocooler. Furthermore, the background of weakly coupled dopants also contributes to the signal, leading to a linear increase on the observed time scale (gray dashed line).

In addition, dephasing may contribute to the damping of Rabi oscillations. To study this, we perform optical spin echo measurements. First, a coherent superposition of the Z_{1-} ground and the Y_{1-} optically excited state is generated by a ±π/2 pulse. Then, a π-pulse cancels the effect of a static detuning between the emitter and the excitation pulse. Last, another π/2 pulse transfers the dopants to the ground or optically excited state, depending on the relative phase. Dephasing will reduce the contrast, i.e., the fluorescence signal difference between measurements with orthogonal phase of the two applied π/2 pulses. In Fig. 3B, we again show exemplary data from a randomly chosen dopant (green triangle in Fig. 2A).

The dephasing times of all eight different emitters we measured (four each at 2 and 6.8 T) are identical within errors, with an average of $T_2 = 0.115(7)$ ms. The corresponding homogeneous linewidth of 2.3 kHz improves by a factor of five with respect to the narrowest single-emitter linewidth reported so far (*14*). Compared to ensemble measurements in the same setup (*22*), the coherence time is slightly reduced. As Er:YSO exhibits a first-order Stark effect, we would not expect that this is an effect of operating at a larger detuning from the center of the inhomogeneous line. Instead, we attribute the broadening to a slightly increased sample temperature caused by the resonator stabilization laser. At lower temperature, lifetime-limited homogeneous linewidth can be achieved at the used resonator parameters (*22*).

Long-term spectral stability

After characterizing the short-term stability of the emitters, we now turn to long-term observations. None of the measured dopants exhibits any signatures of charge instability or blinking that is commonly observed with many other solid-state emitters (*5*, *24*). In Fig. 4A, we again show exemplary data of two well-coupled dopants (orange triangles in Fig. 2A) that are detuned by 5.3 MHz and measured in an alternating sequence without cavity length changes. Only small fluctuations of the emitter frequency are observed between 6-min measurement intervals. The spectral diffusion of both dopants is not correlated, meaning that its source is local to each emitter. We find a standard deviation of the fitted line centers (red) of 45 kHz. Averaging over time (Fig. 4B), we obtain Gaussian lines with 0.14(1)- and 0.16(2)-MHz FWHM (blue).

We performed these long-term measurements on a random sample of six dopants. Over the course of several days, they all give similar temporal behavior to that shown in Fig. 4B. Averaging the measurements, we determine a spectral diffusion linewidth of Γ_{SD} = 0.152(8)-MHz FWHM. This corresponds to an optical Ramsey decay time of $T_2^* = \frac{1}{\pi\Gamma_{SD}} \simeq 2\,\mu s$.

The measured linewidth is much more narrow than that of any previously observed single emitter in any crystalline host (*4*, *15*, *19*, *21*, *24*, *31*). Compared to erbium in the same material in the proximity of interfaces (*10*, *13*), we find an improvement by two orders of magnitude. Compared to other single rare-earth dopants in tailored hosts with no first-order Stark shift (*14*, *20*), a 10-fold narrower line is achieved. Together, these results suggest that our approach of avoiding the proximity to interfaces eliminates the main source of spectral instability encountered in nanophotonic devices.

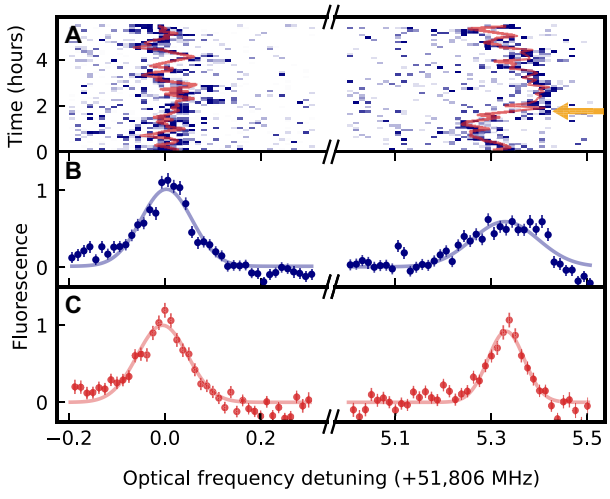

Fig. 4. Long-term spectral stability. Two ions, on resonance with the cavity, are optically excited in an alternating sequence with Gaussian pulses of 0.02-MHz FWHM spectral width. The fluorescence is measured as a function of the excitation laser detuning. (**A**) When the results are averaged over 6-min intervals, the center of the line (red fit results) shows only small fluctuations. Occasional shifts of the center frequency exceeding 0.1 MHz (orange arrow) can be attributed to flips of proximal ^{29}Si nuclear spins. (**B**) When averaging over the full 6-hour measurement record, the Gaussian peaks of the fluorescence exhibit a FWHM of 0.14(1) and 0.16(2) MHz. (**C**) When applying feedforward, i.e., shifting the detuning axis according to the fit center of the last interval to correct for slow frequency shifts, a further linewidth reduction to 0.10(1) MHz (red data and fit) is obtained, depending on the dopant. The error bars denote the 1σ statistical uncertainty.

The observed spectral diffusion linewidth is in good agreement with the expectation from the coupling to the fluctuating bath of yttrium nuclear spins within a few nanometers from each dopant. We calculate this to be 0.20 MHz assuming purely dipolar interactions, which is justified in a large magnetic field, as detailed in (*32*). Thus, a further reduction of the spectral diffusion may be expected with hosts that contain fewer nuclear spins (*33*–*36*).

In the current samples, the absence of other, dominant sources of frequency instability enables the exploration of the dynamics of the frozen core of nuclear spins surrounding individual emitters (*24*). As an example, we observe that some dopants (e.g., the right peak in Fig. 4) show occasional fast shifts of the center frequency exceeding 0.1 MHz (orange arrow in Fig. 4A). We attribute these shifts to flips of proximal ^{29}Si nuclear spins that have a natural isotopic abundance of ~5% and an expected lifetime that is consistent with the observed absence of these shifts over several hours (*26*). The maximum expected ^{29}Si—Er coupling of 0.36 MHz can exceed the measured spectral diffusion linewidth. Thus, our system may enable quantum network nodes with optically interfaced nuclear-spin registers. In turn, undesired nuclear spin–induced shifts may be avoided in isotopically purified samples or by applying a feed-forward operation. To implement the latter, we adapt the detuning of the excitation laser based on the center-frequency fit in the last measurement interval, achieving a further linewidth reduction below 0.10 MHz (in postprocessing) for the dopant shown in Fig. 4C. Using this technique to further reduce the linewidth of all dopants would require faster resonance frequency measurements, ideally within the observed spectral diffusion time scale of 80(20) ms (see Fig. 2C). This may become feasible with further improvements of the experimental setup.

DISCUSSION

In summary, we have shown that the fluorescence of individual emitters in a solid can be enhanced without inducing notable spectral instability by proximal interfaces. The resulting ultranarrow spectral diffusion linewidths enable cavity-enhanced quantum network nodes at a telecommunication wavelength in which hundreds of emitters can be individually controlled via ultradense wavelength-division multiplexing. While our approach is based on erbium dopants in YSO, it can be readily transferred to many other emitters in host crystals that can be polished, etched, or grown to form smooth membranes of a few-micrometer thickness; the most prominent ones are diamond (*21*, *37*), silicon, silicon carbide (*38*, *39*), and a large variety of other semiconductors (*40*), i.e., most of the single-emitter hosts studied so far (*24*).

In our approach, not only the emitter but also the resonator linewidth is narrow. This will enable single-shot spin readout without a cycling transition via frequency-selective fluorescence enhancement (*3*) at low magnetic fields, overcoming the need for emitter-specific, precise field alignment (*13*, *41*). Still, using the built-in piezo to control the cavity resonance, which has a tuning range of several hundred gigahertz, one can switch between all optically resolved dopants and thus increase the number of multiplexed qubits per cavity up to the limit imposed by the inhomogeneous linewidth. Currently, switching is possible on a submillisecond time scale (*42*), which may be further reduced by including electro-optic crystalline layers as host crystal (*15*) or additional tuning element. In addition, using techniques of optimal control (*43*) may allow for exciting one emitter

without exciting others that are close-by in frequency but differ in coupling strength. This can reduce the two-photon component measured in the correlation function of Fig. 2 and may further increase the multiplexing capability of our setup, as it would alleviate the apparent tradeoff that increasing the number of multiplexed emitters reduces the fidelity of single-emitter control.

The narrow homogeneous linewidth, slow spectral diffusion, and high photon generation efficiency of our setup should enable the entanglement of dopants over tens of kilometers of optical fiber via photon interference (*5*) or other, cavity-based protocols that can be less sensitive to slowly fluctuating emitter detuning (*25*). The achieved Purcell enhancement reduces the optical lifetime to $\lesssim$0.5 ms. Thus, after ~30 km, the achievable entanglement rate will not be limited by the time it takes to generate a photon but by the time the photon travels in the fiber. To ensure sufficient ground-state coherence in this setting, one can use hyperfine states of the isotope ^{167}Er (*27*) or host crystals with a low concentration of nuclear spins and erbium impurities (*33*–*36*) to avoid dephasing via spin-spin interactions (*44*).

Over shorter distances, the rate of optical spin-spin entanglement would, however, be limited by the emitter lifetime. This may be further reduced using silicon (*33*, *34*) or other (*36*) host crystals and using Fabry-Perot resonators with higher finesse and smaller mode waist (*45*, *46*). Combining the two, Fourier-limited spectral diffusion linewidth should be achievable, eliminating the need for fast resonance frequency measurements common in solid-state quantum network nodes (*5*, *25*). Last, our setup may allow further steps toward distributed quantum information processing with all-to-all connectivity in a rare earth–based quantum computer (*8*).

MATERIALS AND METHODS

YSO is a commonly used material for the integration of rare-earth dopants toward quantum applications, as it is commercially available with different dopants in a high crystalline quality and its constituents have small nuclear magnetic moments. The Kramers' dopant erbium (*24*) substitutes yttrium in two crystallographic sites. Our study is performed using site 1 that has a transition wavelength of 1536.5 nm and a 414(7)-MHz FHWM Lorentzian inhomogeneous linewidth (*22*) caused by inhomogeneous strain. We use a nominally undoped YSO membrane of 19(1) μm in thickness that contains <1 part per million (ppm) trace impurities of erbium. Even at this low concentration, at the center of the inhomogeneous line, the spectral density of erbium is too high to resolve individual dopants. We therefore operate at several gigahertz detuning, i.e., at a frequency where only few erbium dopants are resonant.

The samples are cooled to <2 K in a closed-cycle cryocooler. We apply an external magnetic field along the *b* axis of the crystal, such that the magnetically inequivalent classes are degenerate with a large effective ground-state *g*-factor of 9 (*26*). The field strength is set to 2.0 or 6.8 T. As the splitting between the Z_1 and Z_2 crystal field levels (>1 THz) and the Zeeman states of the Z_1 manifold (0.3 or 0.9 THz) is much larger than $kT \simeq 0.04$ THz, only the lowest Zeeman level of Z_1 will be occupied. In addition, most paramagnetic impurities are frozen to the ground state, which reduces magnetic noise from electronic spin flips.

To enhance the emission via the Purcell effect, we use a plano-concave Fabry-Perot resonator whose length can be tuned and stabilized to ±1 pm using a piezo tube. To this end, we irradiate a laser at 1593 nm, which is far detuned from the erbium transition but resonant with another longitudinal cavity mode. Depending on its power, the stabilization laser can also lead to a considerable temperature increase (~1 K) of the crystal with respect to the cryostat temperature (*22*).

The device fabrication is described in detail in the supporting information of (*22*). The radius of curvature of the concave mirror, c.f. Fig. 1A, is 155(3) μm. The mirror transmissions are 22(8) ppm (for the flat outcoupling mirror with the bonded crystal) and 20(7) ppm (for the concave mirror), which is comparable to the absorption and scattering losses, 27(14) ppm. This leads to a finesse of $9.0(7) \times 10^4$ and a linewidth of 13(1) MHz. From the independently measured mirror parameters, we expect a Purcell enhancement of $P_{\mathrm{TL}} = 362(26)$ for a two-level system at the maximum of the cavity field. For the investigated transition, with the polarization of the excitation laser and the emitted photons parallel to the D2 axis of the YSO crystal, the branching into other crystal field levels reduces this value to $P = 74(7)$, in good agreement with the measurements. This value is slightly larger than that of our earlier measurements on erbium ensembles (*22*) because of the changed polarization, in combination with an increased mirror separation. This reduces P_{TL} but increases the branching ratio and thus P (*32*).

REFERENCES AND NOTES

1. S. Wehner, D. Elkouss, R. Hanson, Quantum internet: A vision for the road ahead. *Science* **362**, eaam9288 (2018).
2. C. Monroe, J. Kim, Scaling the ion trap quantum processor. *Science* **339**, 1164–1169 (2013).
3. A. Reiserer, G. Rempe, Cavity-based quantum networks with single atoms and optical photons. *Rev. Mod. Phys.* **87**, 1379–1418 (2015).
4. P. Lodahl, S. Mahmoodian, S. Stobbe, Interfacing single photons and single quantum dots with photonic nanostructures. *Rev. Mod. Phys.* **87**, 347–400 (2015).
5. M. Ruf, N. H. Wan, H. Choi, D. Englund, R. Hanson, Quantum networks based on color centers in diamond. *J. Appl. Phys.* **130**, 070901 (2021).
6. H.-J. Briegel, W. Dür, J. I. Cirac, P. Zoller, Quantum repeaters: The role of imperfect local operations in quantum communication. *Phys. Rev. Lett.* **81**, 5932–5935 (1998).
7. N. H. Nickerson, J. F. Fitzsimons, S. C. Benjamin, Freely scalable quantum technologies using cells of 5-to-50 qubits with very lossy and noisy photonic links. *Phys. Rev. X* **4**, 041041 (2014).
8. A. Kinos, Roadmap for rare-earth quantum computing. arXiv:2103.15743 [quant-ph] (29 March 2021).
9. E. Janitz, M. K. Bhaskar, L. Childress, Cavity quantum electrodynamics with color centers in diamond. *Optica* **7**, 1232–1252 (2020).
10. A. M. Dibos, M. Raha, C. M. Phenicie, J. D. Thompson, Atomic source of single photons in the telecom band. *Phys. Rev. Lett.* **120**, 243601 (2018).
11. S. Zaske, A. Lenhard, C. A. Keßler, J. Kettler, C. Hepp, C. Arend, R. Albrecht, W. M. Schulz, M. Jetter, P. Michler, C. Becher, Visible-to-telecom quantum frequency conversion of light from a single quantum emitter. *Phys. Rev. Lett.* **109**, 147404 (2012).
12. C. E. Bradley, J. Randall, M. H. Abobeih, R. C. Berrevoets, M. J. Degen, M. A. Bakker, M. Markham, D. J. Twitchen, T. H. Taminiau, A ten-qubit solid-state spin register with quantum memory up to one minute. *Phys. Rev. X* **9**, 031045 (2019).
13. S. Chen, M. Raha, C. M. Phenicie, S. Ourari, J. D. Thompson, Parallel single-shot measurement and coherent control of solid-state spins below the diffraction limit. *Science* **370**, 592–595 (2020).
14. T. Zhong, J. M. Kindem, J. G. Bartholomew, J. Rochman, I. Craiciu, V. Verma, S. W. Nam, F. Marsili, M. D. Shaw, A. D. Beyer, A. Faraon, Optically addressing single rare-earth ions in a nanophotonic cavity. *Phys. Rev. Lett.* **121**, 183603 (2018).
15. K. Xia, F. Sardi, C. Sauerzapf, T. Kornher, H. W. Becker, Z. Kis, L. Kovacs, D. Dertli, J. Foglszinger, R. Kolesov, J. Wrachtrup, Tunable microcavities coupled to rare-earth quantum emitters. *Optica* **9**, 445–450 (2022).
16. D. M. Lukin, M. A. Guidry, J. Yang, M. Ghezellou, S. D. Mishra, H. Abe, T. Ohshima, J. Ul-Hassan, J. Vučković, Optical superradiance of a pair of color centers in an integrated silicon-carbide-on-insulator microresonator. arXiv:2202.04845 [quant-ph] (10 February 2022).
17. R. M. Macfarlane, Optical Stark spectroscopy of solids. *JOL* **125**, 156–174 (2007).
18. G. Thiering, A. Gali, Ab initio magneto-optical spectrum of group-IV vacancy color centers in diamond. *Phys. Rev. X* **8**, 021063 (2018).

19. M. K. Bhaskar, R. Riedinger, B. Machielse, D. S. Levonian, C. T. Nguyen, E. N. Knall, H. Park, D. Englund, M. Lončar, D. D. Sukachev, M. D. Lukin, Experimental demonstration of memory-enhanced quantum communication. *Nature* **580**, 60–64 (2020).
20. J. M. Kindem, A. Ruskuc, J. G. Bartholomew, J. Rochman, Y. Q. Huan, A. Faraon, Control and single-shot readout of an ion embedded in a nanophotonic cavity. *Nature* **580**, 201–204 (2020).
21. D. Riedel, I. Söllner, B. J. Shields, S. Starosielec, P. Appel, E. Neu, P. Maletinsky, R. J. Warburton, Deterministic enhancement of coherent photon generation from a nitrogen-vacancy center in ultrapure diamond. *Phys. Rev. X* **7**, 031040 (2017).
22. B. Merkel, A. Ulanowski, A. Reiserer, Coherent and Purcell-enhanced emission from erbium dopants in a cryogenic high-Q resonator. *Phys. Rev. X* **10**, 041025 (2020).
23. J. Minář, B. Lauritzen, H. d. Riedmatten, M. Afzelius, C. Simon, N. Gisin, Electric control of collective atomic coherence in an erbium-doped solid. *New J. Phys.* **11**, 113019 (2009).
24. G. Wolfowicz, F. J. Heremans, C. P. Anderson, S. Kanai, H. Seo, A. Gali, G. Galli, D. D. Awschalom, Quantum guidelines for solid-state spin defects. *Nat. Rev. Mater.* **6**, 906–925 (2021).
25. A. Reiserer, Cavity-enhanced quantum network nodes. arXiv:2205.15380 [quant-ph] (30 May 2022).
26. T. Böttger, C. W. Thiel, Y. Sun, R. L. Cone, Optical decoherence and spectral diffusion at 1.5 μm in Er^{3+}: Y_2SiO_5 versus magnetic field, temperature, and Er^{3+} concentration. *Phys. Rev. B* **73**, 075101 (2006).
27. M. Rančić, M. P. Hedges, R. L. Ahlefeldt, M. J. Sellars, Coherence time of over a second in a telecom-compatible quantum memory storage material. *Nat. Phys.* **14**, 50–54 (2018).
28. M. K. Akhlaghi, E. Schelew, J. F. Young, Waveguide integrated superconducting single-photon detectors implemented as near-perfect absorbers of coherent radiation. *Nat. Commun.* **6**, 8233 (2015).
29. C. Becher, A. Kiraz, P. Michler, A. Imamoğlu, W. V. Schoenfeld, P. M. Petroff, L. Zhang, E. Hu, Nonclassical radiation from a single self-assembled InAs quantum dot. *Phys. Rev. B* **63**, 121312 (2001).
30. C. Babin, R. Stöhr, N. Morioka, T. Linkewitz, T. Steidl, R. Wörnle, D. Liu, E. Hesselmeier, V. Vorobyov, A. Denisenko, M. Hentschel, C. Gobert, P. Berwian, G. V. Astakhov, W. Knolle, S. Majety, P. Saha, M. Radulaski, N. T. Son, J. Ul-Hassan, F. Kaiser, J. Wrachtrup, Fabrication and nanophotonic waveguide integration of silicon carbide colour centres with preserved spin-optical coherence. *Nat. Mater.* **21**, 67–73 (2022).
31. A. Faraon, P. E. Barclay, C. Santori, K.-M. C. Fu, R. G. Beausoleil, Resonant enhancement of the zero-phonon emission from a colour centre in a diamond cavity. *Nat. Photonics* **5**, 301–305 (2011).
32. B. Merkel, "Enhancing the emission and coherence of erbium dopants," thesis, Technische Universität München (2021).
33. L. Weiss, A. Gritsch, B. Merkel, A. Reiserer, Erbium dopants in nanophotonic silicon waveguides. *Optica* **8**, 40–41 (2021).
34. A. Gritsch, L. Weiss, J. Früh, S. Rinner, A. Reiserer, Narrow optical transitions in erbium-implanted silicon waveguides. arXiv:2108.05120 [quant-ph] (11 August 2021).
35. M. Le Dantec, M. Rančić, S. Lin, E. Billaud, V. Ranjan, D. Flanigan, S. Bertaina, T. Chanelière, P. Goldner, A. Erb, R. B. Liu, D. Estève, D. Vion, E. Flurin, P. Bertet, Twenty-three–millisecond electron spin coherence of erbium ions in a natural-abundance crystal. *Sci. Adv.* **7**, eabj9786 (2021).
36. P. Stevenson, C. M. Phenicie, I. Gray, S. P. Horvath, S. Welinski, A. M. Ferrenti, A. Ferrier, P. Goldner, S. das, R. Ramesh, R. J. Cava, N. P. de Leon, J. D. Thompson, Erbium-implanted materials for quantum communication applications. *Phys. Rev. B* **105**, 224106 (2022).
37. M. Ruf, M. IJspeert, S. van Dam, N. de Jong, H. van den Berg, G. Evers, R. Hanson, Optically coherent nitrogen-vacancy centers in micrometer-thin etched diamond membranes. *Nano Lett.* **19**, 3987–3992 (2019).
38. B.-S. Song, T. Asano, S. Jeon, H. Kim, C. Chen, D. D. Kang, S. Noda, Ultrahigh-*Q* photonic crystal nanocavities based on 4H silicon carbide. *Optica* **6**, 991–995 (2019).
39. D. M. Lukin, C. Dory, M. A. Guidry, K. Y. Yang, S. D. Mishra, R. Trivedi, M. Radulaski, S. Sun, D. Vercruysse, G. H. Ahn, J. Vučković, 4H-silicon-carbide-on-insulator for integrated quantum and nonlinear photonics. *Nat. Photonics* **14**, 330–334 (2019).
40. J. A. Rogers, M. G. Lagally, R. G. Nuzzo, Synthesis, assembly and applications of semiconductor nanomembranes. *Nature* **477**, 45–53 (2011).
41. M. Raha, S. Chen, C. M. Phenicie, S. Ourari, A. M. Dibos, J. D. Thompson, Optical quantum nondemolition measurement of a single rare earth ion qubit. *Nat. Commun.* **11**, 1605 (2020).
42. B. Casabone, C. Deshmukh, S. Liu, D. Serrano, A. Ferrier, T. Hümmer, P. Goldner, D. Hunger, H. de Riedmatten, Dynamic control of Purcell enhanced emission of erbium ions in nanoparticles. *Nat. Commun.* **12**, 3570 (2021).
43. J. Werschnik, E. K. U. Gross, Quantum optimal control theory. *J. Phys. B: At. Mol. Opt. Phys.* **40**, R175–R211 (2007).
44. B. Merkel, P. Cova Fariña, A. Reiserer, Dynamical decoupling of spin ensembles with strong anisotropic interactions. *Phys. Rev. Lett.* **127**, 030501 (2021).
45. G. Wachter, S. Kuhn, S. Minniberger, C. Salter, P. Asenbaum, J. Millen, M. Schneider, J. Schalko, U. Schmid, A. Felgner, D. Hüser, M. Arndt, M. Trupke, Silicon microcavity arrays with open access and a finesse of half a million. *Light Sci. Appl.* **8**, 37 (2019).
46. D. Najer, I. Söllner, P. Sekatski, V. Dolique, M. C. Löbl, D. Riedel, R. Schott, S. Starosielec, S. R. Valentin, A. D. Wieck, N. Sangouard, A. Ludwig, R. J. Warburton, A gated quantum dot strongly coupled to an optical microcavity. *Nature* **575**, 622–627 (2019).

Acknowledgments

Funding: This project received funding from the European Research Council (ERC) under the European Union's Horizon 2020 research and innovation programme (grant agreement no. 757772) and from the Deutsche Forschungsgemeinschaft (DFG; German Research Foundation) under Germany's Excellence Strategy - EXC-2111 - 390814868. **Author contributions:** All authors contributed to the experimental setup, the measurements, the data analysis, and the writing of the manuscript. **Competing interests:** The authors declare that they have no competing interests. **Data and materials availability:** All data needed to evaluate the conclusions in the paper are present in the manuscript.

Submitted 4 February 2022
Accepted 8 September 2022
Published 26 October 2022
10.1126/sciadv.abo4538